Luminescence and Energy Transfer of the Europium (III) Tungstate Obtained Via the Pechini Method

ARTICLE *in* JOURNAL OF LUMINESCENCE · JANUARY 2003

Impact Factor: 2.72 · DOI: 10.1016/S0022-2313(02)00384-8

Available online at www.sciencedirect.com
SCIENCE DIRECT®
Journal of Luminescence 101 (2003) 11–21
JOURNAL OF LUMINESCENCE
www.elsevier.com/locate/jlumin

Luminescence and energy transfer of the europium (III) tungstate obtained via the Pechini method

C.A. Kodaira[a], H.F. Brito[a,*], O.L. Malta[b], O.A. Serra[c]

[a] *Departamento de Química Fundamental, Instituto de Química da, Universidade de São Paulo, C.P. 26077, 05508-900 São Paulo, SP, Brazil*

[b] *Departamento de Química Fundamental, Universidade Federal de Pernambuco, Cidade Universitária, 50670-901 Recife, PE, Brazil*

[c] *Departamento de Química FFCLRP, Universidade de São Paulo, av. Bandeirantes 3900, 14040-901 Ribeirão Preto, SP, Brazil*

Received 29 October 2001; received in revised form 26 April 2002; accepted 5 June 2002

Abstract

This work presents the preparation of the europium tungstate compound, $Eu_2(WO_4)_3$, through the use of a polymeric precursor according to the Pechini method. In the preparation of this precursor ammonium tungstate, europium nitrate, edta, citric acid and ethylene glycol were mixed and heated at 700°C for 4 h, leading to a luminescent compound. X-ray diffraction, infrared spectroscopy, thermogravimetric analysis and diffuse reflectance spectroscopy were used to characterize the luminescent material. The photoluminescent properties of this compound were studied based on the f^6-intraconfigurational transitions in the spectral range from 250 to 720 nm. When the photoexcitation is monitored into the $O \rightarrow W$ (260 nm) and $O \rightarrow Eu^{3+}$ (310 nm) ligand-to-metal charge-transfer states (LMCT) and $^7F_0 \rightarrow {}^5L_6$ transition of the Eu^{3+} ion (393 nm) the emission spectra present transitions from the $^5D_0$ emitting level at 77 and 298 K. The emission spectra at room temperature, with excitation at the $O \rightarrow W$ and $O \rightarrow Eu^{3+}$ LMCT states, do not present the emission bands from the $^5D_3$, $^5D_2$ and $^5D_1$ emitting levels. On the other hand, the emission spectrum under excitation at the $^7F_0 \rightarrow {}^5L_6$ transition of the Eu^{3+} ion shows narrow emission bands arising from the ^5D_J levels ($J = 1$, 2 and 3). One of the main points of the present study is that this phenomenon is interpreted on the basis of a resonance crossover between the LMCT states and the ^5D_J levels ($J = 1$, 2 and 3). The emission quantum efficiency of the Eu^{3+} ion in this system is also discussed.

Keywords: Europium ion; Pechini method; Tungstate; Photoluminescence; LMCT states

1. Introduction

The research on the luminescent materials containing trivalent rare earth ions (RE^{3+}) has increased considerably in the last three decades [1–3]. Major applications are in emissive displays and fluorescent lamps. In addition, some X-ray detector systems are based on luminescent materials as well. Quite a few of these materials also found their way into applications. In many cases, rare earth phosphors noticeably improved the performance of the devices.

The photoluminescent properties of the Eu^{3+} and Tb^{3+} ions make them potential candidates for

*Corresponding author. Tel.: +55-11-3818-3708; fax: +55-11-3815-5579.

E-mail address: hefbrito@iq.usp.br (H.F. Brito).

0022-2313/03/$ - see front matter © 2002 Published by Elsevier Science B.V.
PII: S0022-2313(02)00384-8

use as luminescent materials [4–8]. However, the europium ion provides additional facilities in the interpretation of the spectral data as compared to the terbium ion. The Eu^{3+} ion has a great advantage because it has non-degenerate ground and emitting states and the $^5D_0 \rightarrow {}^7F_0$ transition gives information about the impurity or if this ion occupies more than one site symmetry, particularly of the type C_{nv}, C_n, or C_s. The intensity of the $^5D_0 \rightarrow {}^7F_1$ transition (allowed by magnetic dipole) is formally insensitive to the crystal field environment and consequently can be used as a reference transition.

Inorganic luminescent materials containing rare earth ions usually present very intense absorption bands in the ultraviolet region consistent with allowed interconfigurational transitions, $4f^N \rightarrow 4f^{N-1}5d$, and with ligand-to-metal charge-transfer states (LMCT), that may mask the forbidden narrow intraconfigurational $4f^N \rightarrow 4f^N$ transitions [1,9]. The LMCT states depend on: (a) the distance between the metal ion and ligands—this transition shifts toward lower energy when the bond length increases, (b) the optical electronegativity (χ_{opt})—the electronegativity of a ligand can alter the position of the LMCT states, becoming very helpful to predict the energy of this transition in different chemical environments and (c) the electroaffinity of the rare earth ion where the LMCT state corresponds to a reduction $4f^N \rightarrow 4f^{N+1}L^{-1}$, whereas the RE^{3+} ions gain one electron, for example: the Eu^{3+} ions ($4f^6$) tend to reduce in order to obtain the half-filled stable shell configuration [9].

McDonald et al. [10] were the first to report the europium tungstate preparation from Eu_2O_3 at 1000°C and to study its luminescent properties. Borchardt [11] prepared the europium tungstate with similar purposes and Templeton and Zalkin [12] studied the crystal structure of $Eu_2O_3 \cdot 3WO_3$. Since then, some different ways were used to synthesize the europium tungstate, but always involving high temperatures and/or a long time of heating. In the last decade, several low temperature preparation techniques have been used to prepare fine particle systems such as co-precipitation [13], sol–gel method [14] and hydrothermal synthesis [15].

In this paper, we have used the Pechini method [16–20] to prepare the $Eu_2(WO_4)_3$ compound. This technique known due to the low cost and versatility is a low temperature synthetic method that uses the dissolution of cations in an aqueous citric acid (CA) solution. Ethylene glycol (EG) addition promotes polymerization (esterification). After polymerization the segregation of cations during thermal decomposition is minimal, owing to the formation of high viscosity polyester. Besides the preparation of the $Eu_2(WO_4)_3$, we also investigated its photoluminescent properties, which have not been reported in the literature. An emission quenching phenomenon observed for the $^5D_{1,2,3}$ manifolds, under excitation at the LMCT states, is here discussed and interpreted as a resonance crossover between the LMCT states and the $^5D_{1,2,3}$ levels. The relatively low emission quantum efficiency (19%) for the $^5D_0$ level, as compared to the $K_5Eu_2(WO_4)_{5.5}$ compound, is interpreted as a partial quenching also due to the LMCT states.

2. Experimental section

2.1. Preparation and measurements

The $RE_2(WO_4)_3$ compounds (RE^{3+} = Eu and Gd) were prepared by the Pechini method [16–20]. The starting materials were ammonium tungstate (99.999%, Acros), europium and gadolinium nitrates—synthesized from RE_2O_3 (99.9%, Aldrich), ethylene glycol (99.5%, Merck) and citric acid (99.5%, Merck). First, the ammonium tungstate was dissolved in heated aqueous solution (~60°C) adjusting the pH at ~7.0 with ammonium hydroxide and nitric acid. Second, aqueous solutions of the rare earth nitrate and ammonium tungstate in the molar ratio 2:3 (RE^{3+}:WO_4^{2-}) were mixed with continuous stirring which produced an insoluble precipitate of the rare earth tungstate. Subsequently, the ethylenediaminetetraacetic acid (EDTA) was added to this mixture and the stable complex of RE^{3+} ion was formed while the WO_4^{2-} remained in the solution, in this step the pH ~ 5 was adjusted with ammonium acetate [21]. To this clear solution citric acid and

ethylene glycol were added, under continuous stirring and heating in water bath, to form the polymeric resin, adjusting the pH to ~ 5 with ammonium acetate. The brown transparent glassy resin was heated at 450°C for 2 h, resulting in a fluffy black mass, which was ground into a powder (precursor). The next step consisted in the calcination of this precursor at 700°C for 4 h producing the $RE_2(WO_4)_3$ as a white powder.

The X-ray diffraction patterns were obtained on a Philips diffractometer model X'PERT-MPD using CuKα radiation (40 kV and 40 mA) in the interval of 2° to 70° (2θ) and 1 s of pass time, using the powder XRD method.

Thermogravimetric (TG) and derivative thermogravimetric (DTG) curves were obtained with a TG-50 thermobalance (Shimadzu), using platinum crucibles with 2.7 mg of the sample, under dynamic condition of air atmosphere (50 ml min^{-1}), at heating rate of 10°C min^{-1}.

The Raman spectrum was obtained in a Renishaw system 3000 equipment, which comprises a single monochromator (0.25 m focal distance), a holographic grating (1800 grooves mm^{-1}) and a Peltier cooled CCD detector (600×400 pixels). The equipment is fitted with an Olympus metallurgical microscope and the sample was investigated on a microscope slide with an $\times 80$ lens. The spectrum was obtained at room temperature in the spectral range of 1200–100 cm^{-1}, with the 488 nm line of an argon ion laser (Spectra Physics) and the laser power was kept at 40 μW.

Infrared data were recorded on a Bomem MB 100 spectrometer by averaging 96 scans with a resolution of 4 cm^{-1}. Samples were physically mixed with KBr and pressed into self-supporting wafer. These measurements were made at room temperature in the range of 1200–450 cm^{-1}.

The diffuse reflectance spectra, at room temperature, were recorded in a Shimadzu model UV-2401PC spectrophotometer equipped with an integration sphere ($BaSO_4$ from Waco Pure Chemicals was used to dilute the solid sample).

The excitation and emission spectra at room and liquid nitrogen temperature were collected at an angle of 22.5° (front face) in a spectrofluorimeter (SPEX-Fluorolog 2) with double grating 0.22 m monochromators (SPEX 1680), a 450 W Xenon lamp as the excitation source. This apparatus was controlled by a spectroscopy computer DM3000F. The solid samples were maintained in a quartz dewar flask at 77 K. The lifetime measurements were recorded at 298 K using the phosphorimeter (SPEX 1934D) accessory coupled with the spectrofluorimeter.

3. Results and discussion

3.1. Characterization

The XRD pattern of the powder $Eu_2(WO_4)_3$ obtained after heating the precursor at 700°C showed characteristic lines of standard compound with a monoclinic (pseudo-orthorhombic) lattice [12], according to the JCPDS card #22–287 (omitted figure). It is noted the absence of the peaks assigned to the europium oxide and WO_3 group, which indicates that the $Eu_2(WO_4)_3$ compound was obtained in a pure form.

Fig. 1 shows the TG/DTG curves of the precursor powder that were obtained after heating the polymeric resin at 200°C for 2 h. The weight loss of 3.4% in the range from 25°C to 200°C was associated to water loss. The decomposition of organic constituents showed weight loss of 77.3% in the temperature interval from 200°C to 700°C. Consequently, the TG analysis indicated that the formation of the europium tungstate occurs around 700°C temperature, taking in account that in the interval from 700°C until 900°C no weight loss was observed. It indicates that the $Eu_2(WO_4)_3$ compound is obtained at lower temperature (about 700°C), using the Pechini method, than those solid-state reactions with heating above 900°C [10,22,23]. From the DTG curve, several overlapped events assigned to the decomposition of the organic constituents can be observed.

Previous structural study [23] reports that rare earth tungstates of general formula $RE_2(WO_4)_3$, where RE^{3+} = La–Dy, have similar vibrational spectra due to their similar structures. Therefore, IR and Raman data for the $Eu_2(WO_4)_3$ compound obtained in this work were compared with those of $Ce_2(WO_4)_3$ and $La_2(WO_4)_3$ reported in Ref. [24], suggesting a T_d point group symmetry. These

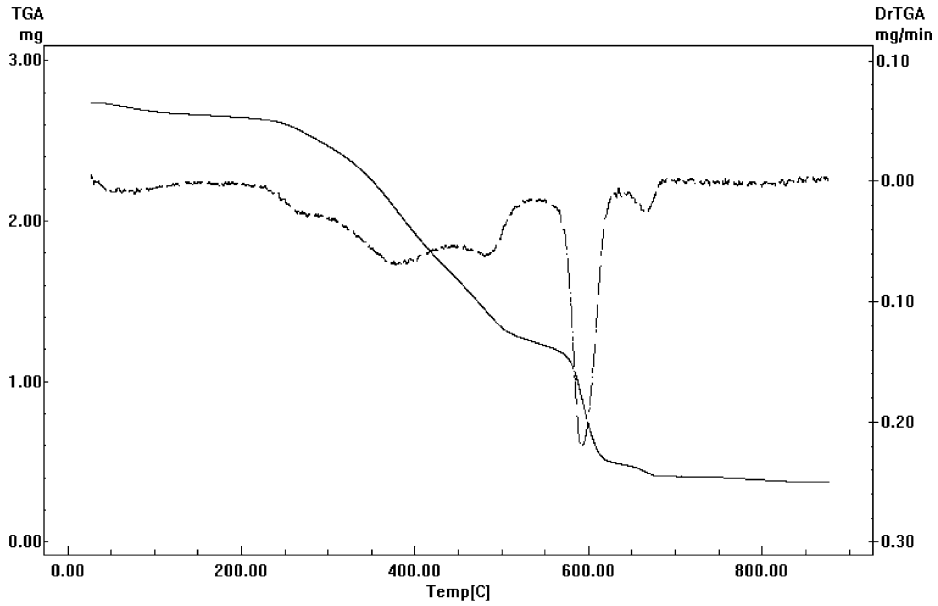

Fig. 1. TG curve of the $Eu_2(WO_4)_3$ precursor powder in air flow of 50 ml min^{-1}.

compounds showed two non-equivalent WO_4 units, while the $Eu_2(WO_4)_3$ compound contains only one type of WO_4 unit. This fact can be corroborated by the presence of the very strong bands around 925 and 950 cm^{-1} assigned to the symmetric stretching of WO_4 shown in the Raman and IR spectra, respectively.

Fig. 2 shows the diffuse reflectance spectrum of the powdered sample of the $Eu_2(WO_4)_3$ compound recorded in the spectral region from 250 to 800 nm at room temperature. This compound exhibits the high intensity broad band in the UV region around 265 nm assigned to the absorption of the $O \rightarrow W$ LMCT state. On the other hand, the inset in Fig. 2 presents the amplified spectrum in the range from 320 to 700 nm, also showing narrow absorption lines characteristic of the $4f^6$-intraconfigurational transitions arising from the trivalent europium ion. The $^7F_0 \rightarrow {}^5D_J$ transitions present low intensity absorption bands since they are forbidden by Laporte rule, while the higher intensity $O \rightarrow W$ band is an electronically allowed transition (LMCT state).

3.2. Photoluminescent study

The excitation and emission spectra of the $Gd_2(WO_4)_3$ compound obtained at 77 K are shown in Fig. 3, where the excitation band has a maximum at about 265 nm. The intense broad emission band lies between 400 and 700 nm with a maximum at about 505 nm corresponding to charge transfer transition between the O^{2-} anion and the W^{6+} cation. The use of trivalent gadolinium ion is due to the absence of emission bands in the visible region because of the large energy gap ($\sim 32000\ cm^{-1}$) between the $^8S_{7/2}$ ground state and first $^6P_{7/2}$ excited state [25].

The excitation and emission spectra illustrated in Fig. 3 present a large Stokes shift for the tungstate group. The excitation spectra of the $Gd_2(WO_4)_3$ compound were obtained under emissions at 425, 505 and 624 nm wavelengths (Fig. 3a), presenting similar profiles. These bands are assigned to the tungstate group (WO_4^{2-}) LMCT, which corroborates with the results obtained from the reflectance spectrum

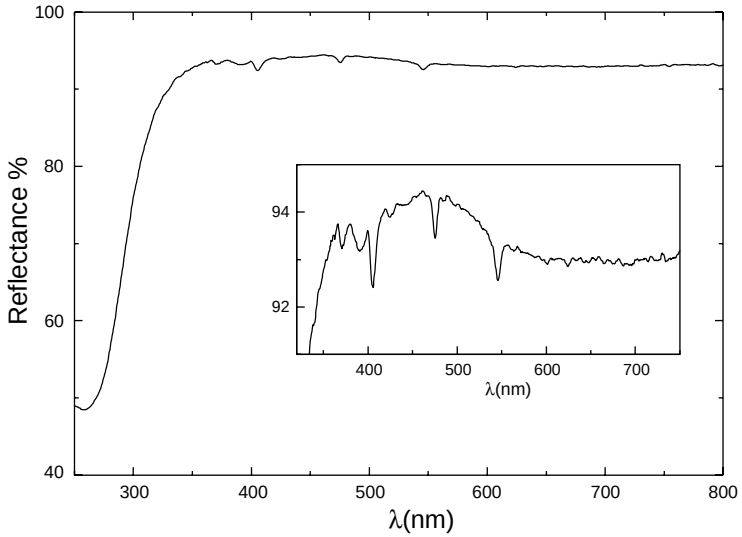

Fig. 2. Diffuse reflectance spectrum of $Eu_2(WO_4)_3$ at room temperature, in the solid state. The inset shows the amplified spectrum in the range from 320 to 700 nm.

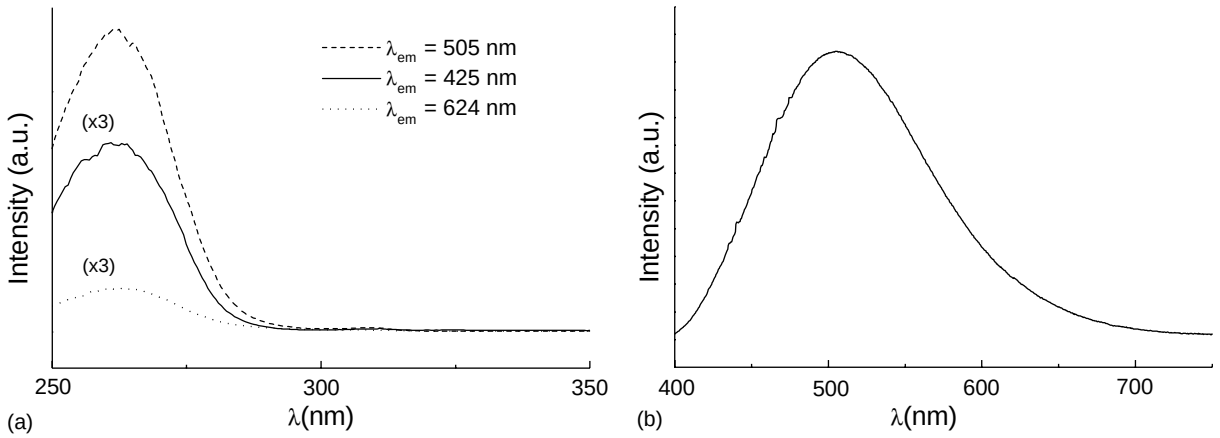

Fig. 3. Luminescence spectra of the WO_4^{2-} in $Gd_2(WO_4)_3$ compound at 77 K: (a) excitation spectra recorded in the range from 250 to 300 nm under emission at 425 nm (solid line), 500 nm (dash line) and 650 nm (dot line) and (b) emission spectrum obtained in the range from 400 to 700 nm when excited at 260 nm.

(Fig. 2). The above results indicated the presence of only one WO_4^{2-} species in this system, different from those data obtained by Blasse et al. [26], which presented two different excitation spectra suggesting two different WO_6^{2-} components.

The excitation spectrum of the europium tungstate compound in Fig. 4 was obtained at liquid nitrogen temperature in the spectral range from 250 to 590 nm under emission at 614.8 nm. A broad low intensity band is noticed in the range 250–320 nm corresponding to the LMCT states from the $O \rightarrow W$ and $O \rightarrow Eu^{3+}$ transitions at around 265 and 310 nm, respectively. It is also noted in Fig. 4 that the LMCT bands are enveloped with the sharp lines at around 298, 302 and 317 nm, corresponding to the $^7F_0 \rightarrow {}^5F_{2,4}$

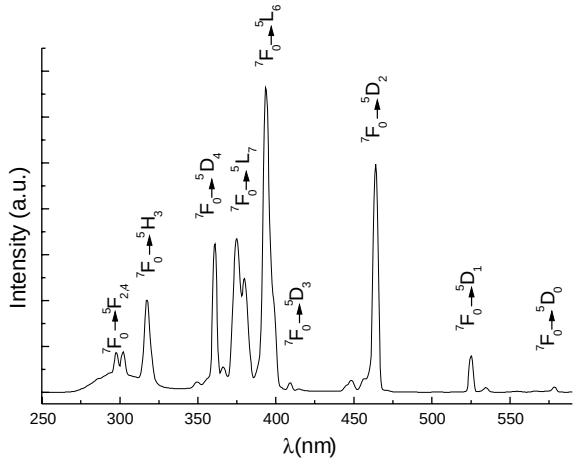

Fig. 4. Excitation spectrum of the $Eu_2(WO_4)_3$ compound with emission monitored at 614.8 nm at liquid nitrogen temperature.

and $^5H_3$ transitions from the Eu^{3+} ion. As can be seen, the excitation spectrum presents shape lines consistent with the $^7F_0 \rightarrow {}^5L_J$ ($J = 0-7$) transitions of the Eu^{3+} ion (Table 1) [27–30].

Fig. 5 shows the emission spectra of the $Eu_2(WO_4)_3$ compound in the range from 420 to 570 nm at room temperature and 77 K, under excitation at 260, 310 and 393 nm. The emission spectra (Figs. 5a and b) recorded at room temperature, with excitation at the $O \rightarrow W$ LMCT from the WO_4^{2-} group and the $O \rightarrow Eu^{3+}$ LMCT, at 260 and 310 nm, respectively, do not present the emission bands from the $^5D_3$, $^5D_2$ and $^5D_1$ levels. On the other hand, the emission spectrum (Fig. 5c) with excitation into the $^7F_0 \rightarrow {}^5L_6$ transition of the Eu^{3+} ion ($\sim$393 nm) shows narrow emission bands arising from these ^5D_J levels ($J = 3$, 2 and 1). According to Fonger and Struck [31], this phenomenon occurs due to a resonance crossover between the $O \rightarrow W$ and $O \rightarrow Eu^{3+}$ LMCT states and the ^5D_J emitting levels ($J = 3$, 2 and 1) near the LMCT band minimum considering that the low lying of the LMCT state skips the higher lying ^5D_J emitting levels during its relaxation process [1,26] (Fig. 6).

The emission spectrum under excitation into the $^7F_0 \rightarrow {}^5L_6$ transition (Fig. 5f), at low temperature presents bands arising from the ^5D_J levels ($J = 3$, 2 and 1) with higher resolution than at room temperature (Fig. 5c). Additionally, the emission

Table 1
Transition energies of the $^5D_J \rightarrow {}^7F_{J''}$ manifolds (in cm^{-1}) observed in the excitation spectra of the $Eu_2(WO_4)_3$ compound at liquid nitrogen temperature

Transition	(cm^{-1})
$^7F_0 \rightarrow {}^5F_4$	33557
$^7F_0 \rightarrow {}^5F_2$	33113
$^7F_0 \rightarrow {}^5H_3$	31546
$^7F_0 \rightarrow {}^5D_4$	28571 28129 27700 27322
$^7F_0 \rightarrow {}^5L_7$	26666 26315
$^7F_0 \rightarrow {}^5L_6$	25413 25062
$^7F_0 \rightarrow {}^5D_3$	24449 24096
$^7F_0 \rightarrow {}^5D_2$	22421 22296 21889 21552
$^7F_0 \rightarrow {}^5D_1$	19048 18695
$^7F_0 \rightarrow {}^5D_0$	17286

from the $^5D_3$ is extremely weak at room temperature and the $^5D_2$ remaining emissions are not well characterized. However, a strong component from the $^5D_1$ level is observed. On the other hand, the emission spectrum (Fig. 5d) recorded at 77 K with excitation monitored at the $O \rightarrow W$ LMCT states (260 nm) shows only the transition from the emitting $^5D_1$ level. Such process is related to the feeding of the $O \rightarrow W$ and $O \rightarrow Eu^{3+}$ LMCT states upon excitation into the 4f states, which shifts the ^5D_J ($J = 3$, 2 and 1) population to the lower $^5D_0$ emitting level and leads to a luminescence quenching in the following order $^5D_3 > {}^5D_2 > {}^5D_1 > {}^5D_0$ with increasing temperature [31] (Fig. 6). In the case of the emission spectrum (Fig. 5e) recorded at 77 K, under excitation into the $O \rightarrow Eu^{3+}$ LMCT

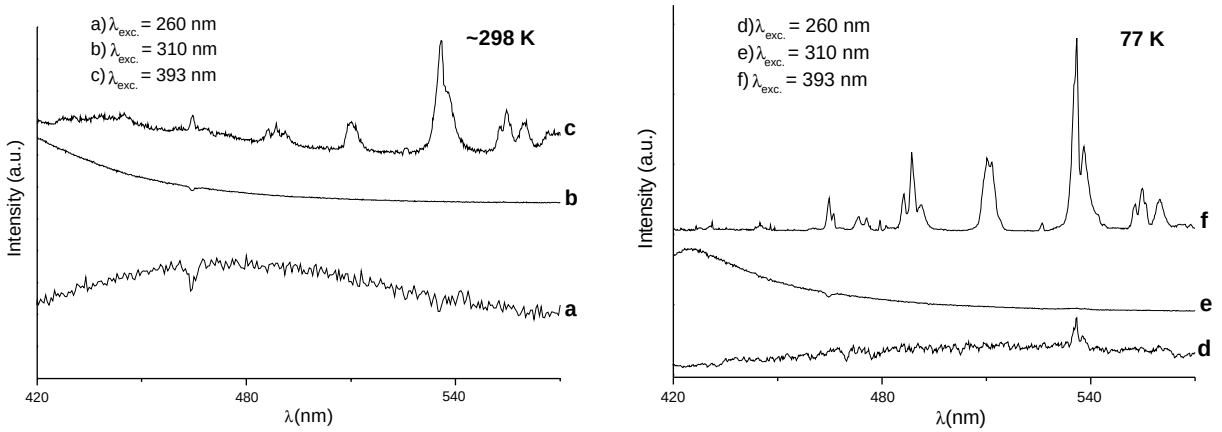

Fig. 5. Emission spectra of the $Eu_2(WO_4)_3$ compound, at 298 and 77 K temperature with excitations monitored at: (a) and (d) $O \rightarrow W$ LMCT band around 260 nm; (b) and (e) $O \rightarrow Eu^{3+}$ LMCT band around 310 nm; (c) and (f) $^5L_6$ level of the Eu^{3+} ion at 393 nm.

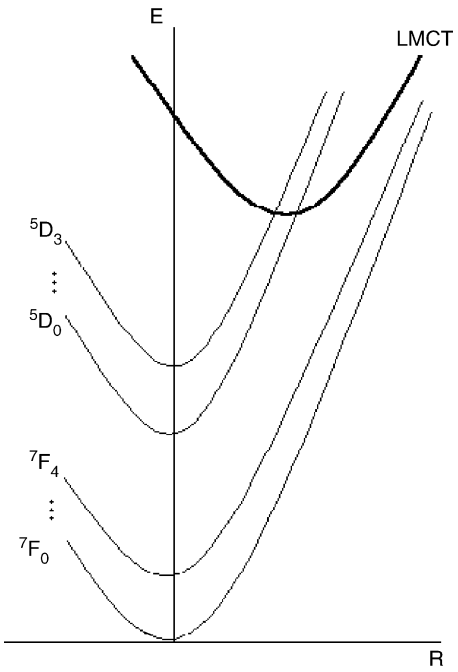

Fig. 6. Schematic configurational coordination diagram for the ground (^7F_J), emitting (^5D_J) and LMCT states for the $Eu_2(WO_4)_3$ compound. The borderline curve shows qualitatively the position of the $O \rightarrow Eu^{3+}$ LMCT state, which feeds the emitting (^5D_J) levels. Only a few parabolas of the $4f^6$ configuration have been drawn.

states, the 4f–4f transitions are not observed suggesting that this quenching process occurs even at liquid nitrogen temperature.

Fig. 7 shows the emission spectrum of the europium tungstate prepared at 700°C, recorded at 77 K, with emissions corresponding to the $^5D_J \rightarrow {}^7F_{J'}$ electronic transitions (where $J = 0-3$ and $J' = 0-4$) in the range of 420–720 nm (see Table 2), under excitation at 393 nm. It is noted that the emission spectrum at room temperature shows the same spectral profile with lower resolution when compared to that obtained at 77 K, which indicates that there are no structural changes in the compound when the temperature is lowered.

Based on the number of bands corresponding to the $^5D_0 \rightarrow {}^7F_0$ transition observed around 579.8 nm (Fig. 7), the presence of only one peak suggests the existence of one local site symmetry for the Eu^{3+} ion chemical environment. Another argument that agrees with the presence of one-site symmetry around Eu^{3+} ion is the mono-exponential behavior in the luminescence decay curve of the emitting $^5D_0$ level. The lifetime measurement for the $^5D_0$ excited state of the rare earth metal ion recorded at room temperature shows a short radiative lifetime τ at about 0.180 ms (Table 3).

The photoluminescence investigation carried out on the $^5D_0 \rightarrow {}^7F_1$ transition in the range from 590 to 600 nm (Fig. 6), shows three peaks around 591.0, 592.0 and 594.6 nm, indicating that the rare earth ion is found in only one type of local chemical environment. The radiative rate of the $^5D_0 \rightarrow {}^7F_1$ transition, allowed by magnetic dipole,

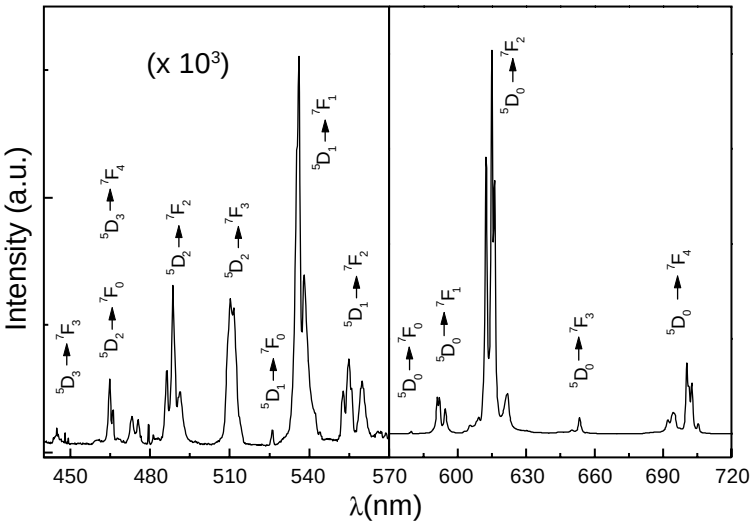

Fig. 7. Emission spectrum of the $Eu_2(WO_4)_3$ compound with excitation monitored at 393 nm at liquid nitrogen temperature.

Table 2
Transition energies of the $^5D_J \rightarrow {}^7F_{J'}$ manifolds (in cm^{-1}) observed in the emission spectra of the $Eu_2(WO_4)_3$ at 77 K

Transition	Energy	Transition	Energy	Transition	Energy
$^5D_3 \rightarrow {}^7F_3$	22472	$^5D_2 \rightarrow {}^7F_3$	19600	$^5D_0 \rightarrow {}^7F_2$	16329
	22452		19546		16260
	22321		19516		16228
	22262		19455		16087
$^5D_2 \rightarrow {}^7F_0 + {}^5D_3 \rightarrow {}^7F_4$	21729	$^5D_1 \rightarrow {}^7F_0$	19011		
	21692			$^5D_0 \rightarrow {}^7F_3$	15868
	21514	$^5D_1 \rightarrow {}^7F_1$	18685		15713
	21450		18657		15596
	21413		18587		15513
	21331				15385
	21276	$^5D_1 \rightarrow {}^7F_2$	18089		15305
			18024		15230
$^5D_2 \rightarrow {}^7F_1$	21133		17992		
	21035		17883	$^5D_0 \rightarrow {}^7F_4$	14451
	20859		17863		14401
					14388
$^5D_2 \rightarrow {}^7F_2$	20781	$^5D_0 \rightarrow {}^7F_0$	17247		14339
	20559				14277
	20467	$^5D_1 \rightarrow {}^7F_3$	17129		14261
	20433				14233
	20383	$^5D_0 \rightarrow {}^7F_1$	16920		14176
	20350		16892		
			16818		

is almost independent of the crystal field environment around the europium ion. Consequently, it can be taken as a standard transition in order to determine the radiative rates.

The luminescence spectrum in Fig. 7 also displays the most intense emission band assigned to the hypersensitive $^5D_0 \rightarrow {}^7F_2$ transition, that splits in four bands. According to Macalik et al. [29], the

Table 3
Experimental intensity parameters (Ω_λ), emission quantum efficiency (η), lifetimes (τ), non-radiative (A_{nrad}), radiative (A_{rad}) and total (A_{total}) rates for the $Eu_2(WO_4)_3$, $[Eu(TTA)_3(H_2O)_2]$ and EuY–V compounds, at room temperature. The R_{02} parameter is the ratio between the intensities of the $^5D_0 \rightarrow {}^7F_0$ and $^5D_0 \rightarrow {}^7F_2$ transitions

Compounds	A_{rad} (s^{-1})	A_{nrad} (s^{-1})	A_{total} (s^{-1})	Ω_2 (10^{-20} cm^2)	Ω_4 (10^{-20} cm^2)	R_{0-2}	τ (ms)	η(%)	Ref.
$Eu_2(WO_4)_3$	1048	4477	5525	26.9	12.8	0.0013	0.180	19	[a]
EuY–V	—	—	—	9.5	6.4	0.0019	0.43–3.5	—	[41]
$[Eu(TTA)_3(H_2O)_2]$	1110	2730	3846	33.0	4.6	0.0130	0.260	29	[34]

[a] This work.

weak sidebands accompanying the $^5D_0 \rightarrow {}^7F_2$ transition are of vibronic origin. This result also suggests a unique crystallographic site for the Eu^{3+} ion compared with the RE^{3+} ions in $AgREW_2O_8$ [32].

A careful analysis of the emission spectrum under excitation at 393 nm in Fig. 7 reveals the absence of the broad band assigned to the O→W LMCT state as illustrated in Fig. 3. This indicates that the tungstate group transfers energy efficiently for the rare earth ion.

3.2.1. Intensity parameters

The standard theory of 4f–4f intensities gives the integrated coefficient of spontaneous emission (radiative) of a transition between two manifolds J and J' [33]. The Ω_λ experimental intensity parameters for $J-J'$ transitions contain the contributions from the forced electric dipole and dynamic coupling mechanisms. They can be estimated theoretically from structural data or determined experimentally from absorption or emission spectra.

It is important to study the influence of the tungstate anion on the europium luminescence behavior by determining the radiative contribution for the depopulation of the emitting level, $^5D_0$, and consequently for the emission quantum efficiency. In this case we have to consider the spectral data at room temperature using the $^5D_0 \rightarrow {}^7F_2$ and $^5D_0 \rightarrow {}^7F_4$ transitions of the Eu^{3+} ion to determine the $\Omega_\lambda(\lambda = 2$ and 4) experimental intensity parameters by taking the $^5D_0 \rightarrow {}^7F_1$ transition as the reference. The emission intensity, $I = \hbar\,\omega A\,N$, is expressed in terms of the surface under the emission curve, where $\hbar\,\omega$ is the transition energy, N is the population of the emitting level ($^5D_0$) and the Einstein's coefficient of spontaneous emission [33–37], A, in this case may be given by

$$A_{0-\lambda} = \frac{4e^2\omega^3}{3\hbar c^3}\chi \sum_{\lambda=2,4} \Omega_\lambda \left\langle {}^5D_0 \left\| U^{(\lambda)} \right\| {}^7F_J \right\rangle^2, \tag{1}$$

where $\chi = n_0(n_0^2+2)^2/9$ is a Lorentz local field correction. The square reduced matrix elements are $\left\langle {}^5D_0 \left\| U^{(2)} \right\| {}^7F_2 \right\rangle^2 = 0.0032$ and $\left\langle {}^5D_0 \left\| U^{(4)} \right\| {}^7F_4 \right\rangle^2 = 0.0023$ in Eq. (1) [38], and an average index of refraction equal to 1.5 was used. In this case the $A_{0-\lambda}$ values are obtained by using the relation:

$$A_{0-\lambda} = A_{0-1}\frac{S_{0-\lambda}}{S_{0-1}}\frac{\sigma_\lambda}{\sigma_1}, \tag{2}$$

where $S_{0-\lambda}$ is the area under the curve related to the $^5D_0 \rightarrow {}^7F_\lambda$ transition obtained from the spectral data, σ_λ is the energy barycenter of the $0-\lambda$ transition and A_{0-1} is the Einstein's coefficient for the 0–1 magnetic dipole transition. The A_{01} value is estimated to be around of $50\,s^{-1}$ [33]. The Ω_6 intensity parameter was not included in this calculation since the $^5D_0 \rightarrow {}^7F_6$ transition could not be observed.

The lifetime (τ), non-radiative (A_{nrad}) and radiative (A_{rad}) rates are related through the following equation

$$A_{tot} = \frac{1}{\tau} = A_{rad} + A_{nrad}, \tag{3}$$

where the A_{rad} rate was obtained by summing over the radiative rates A_{0J} for each $^5D_0 \rightarrow {}^7F_J$ transitions is given by

$$A_{rad} = \sum_J A_{0J}. \tag{4}$$

The emission quantum efficiency of the emitting $^5D_0$ level is given by

$$\eta = \frac{A_{rad}}{A_{rad} + A_{nrad}}. \tag{5}$$

In Table 3 the values of the Ω_λ intensity parameters ($\lambda = 2$ and 4) are shown for the $Eu_2(WO_4)_3$, EuY zeolite incorporated with vanadium [41] and $[Eu(TTA)_3(H_2O)_2]$ [34] compounds, where TTA = thenoyltrifluoroacetonate. When a comparison is made between the Ω_2 parameters for all the compounds, the highest value ($33.0 \times 10^{-20}\,cm^2$) for the Eu-(TTA)-complex is noted, which indicates the highest hypersensitive behavior of the $^5D_0 \rightarrow {}^7F_2$ transition. Consequently, the Eu^{3+} ions in the tungstate and zeolitic systems are in a lesser polarizable environment than in $[Eu(TTA)_3(H_2O)_2]$ complex, suggesting a smaller electric dipole character to the $^5D_0 \rightarrow {}^7F_2$ transition for the zeolite systems. Nevertheless the europium ion in the $Eu_2(WO_4)_3$ compound is in a more polarizable environment than in the EuY–V sample due to the values of Ω_2 parameters are 26.9 and $9.5 \times 10^{-20}\,cm^2$, respectively. This indicates a considerable covalent character of the metal–donor atom interaction in the europium tungstate compound.

Table 3 shows the Ω_4 experimental intensity parameter values presenting the highest for the $Eu_2(WO_4)_3$ compound. It is known that the Ω_2 parameter depends rather on the lower rank components of the crystal field and dynamic coupling interactions, while the Ω_4 parameter depends rather on the corresponding higher components. In the tungstate system $\Omega_2 > \Omega_4$ parameters suggests that the coordination geometry is such that the higher rank components of these interactions have lesser values than the lower rank ones. Therefore this might suggest that the site symmetry occupied by the Eu^{3+} ion does not have a character of centrosymmetric chemical environment considering that the $^5D_0 \rightarrow {}^7F_2$ transitions is formally forbidden due to the electric dipole selection rule. The compound also shows a high value for the Ω_4 parameter ($12.8 \times 10^{-20}\,cm^2$) indicating the high sensitive behavior of the $^5D_0 \rightarrow {}^7F_4$ transition possibly as a consequence of the basicity of the oxygen donor.

As reported in Ref. [39], the $K_5Eu_x(WO_4)_{2.5+1.5x}$ compound ($x = 0.5-3.0$) shows a highly efficient red emission with almost no concentration quenching due to its crystal structure (scheelite-like tetragonal structure) which shows a spatial distribution of Eu-O-W-O-Eu bands that blocks energy transfer between Eu^{3+} ions. The $Eu_2(WO_4)_3$ compound presents a low emission quantum efficiency ($\eta = 19\%$) while the $K_5Eu_2(WO_4)_{5.5}$ compound shows 54%. This difference can be explained in terms of the $O \rightarrow Eu^{3+}$ LMCT states that populate, at least partially the ^7F_J ground states of the Eu^{3+} ion (Fig. 6), therefore the luminescence is strongly suppressed [1,40].

The R_{0-2} experimental intensity parameter is the ratio between the intensities of the $^5D_0 \rightarrow {}^7F_0$ and $^5D_0 \rightarrow {}^7F_2$ transitions. The R_{02} parameter may give information on the *J*-mixing effect associated with the $^5D_0 \rightarrow {}^7F_0$ transition [37]. In this case, this effect is mainly due to the mixing between the $^7F_2$ manifold and the $^7F_0$ level through the rank-two components of the crystal field. The $Eu_2(WO_4)_3$ and EuY–V systems show a much smaller R_{02} values than the $[Eu(TTA)_3(H_2O)_2]$ complex suggesting a much lower magnitude of the *J*-mixing effect (Table 3).

4. Concluding remarks

The $Eu_2(WO_4)_3$ compound was prepared using the Pechini method that produces a phase-pure at reduced temperature in contrast to the conventional solid-state preparation. The diffuse reflectance data shows the absorption of the $O \rightarrow W$ LMCT state and the sharp lines corresponding to the Eu^{3+} ion. The infrared and Raman spectra indicated only one type of WO_4 tetrahedron. The $^5D_0 \rightarrow {}^7F_0$ transition showed one peak assigned and a mono-exponential for the decay curve of emitter $^5D_0$ level indicate the presence of only one Eu^{3+} site in the chemical environment. The emission spectra under excitation at the LMCT states ($O \rightarrow W$ and $O \rightarrow Eu^{3+}$) show only transitions from the emitter $^5D_0$ level whereas under excitation at $^7F_0 \rightarrow {}^5L_6$ transition of the Eu^{3+} ion show transitions arising from emitter $^5D_3$, $^5D_2$, $^5D_1$ and $^5D_0$ levels. This phenomenon occurs due to a resonance crossover between the LMCT states and the emitter ^5D_J levels. It is interpreted as a feeding of $O \rightarrow W$ and $O \rightarrow Eu^{3+}$ LMCT states upon excitation into the 4f states, leading to the quenching process that follows the order

$^5D_3 > {}^5D_2 > {}^5D_1 > {}^5D_0$ with increasing temperature. The $Eu_2(WO_4)_3$ compound presents higher value of the Ω_2 parameter compared as EuY–V zeolite system but it has lesser value than Eu-TTA-complex which reflects a highly polarizable chemical environment around the Eu^{3+} ion in the complex. The rather low value found for the R_{02} parameter indicates a rather weak *J*-mixing effect, in comparison with the $[Eu(TTA)_3(H_2O)_2]$ complex.

Acknowledgements

We thank the Brazilian agencies FAPESP and CNPq (RENAMI) for financial support. We also thank Dr. A.C.V. Coelho and V.F.J. Kozievitch from the Departamento de Engenharia Química da Escola Politécnica (USP) for XRD pattern recording, Dr. D.L.A. Faria from the Laboratório de Espectroscopia Molecular (IQ-USP) for the Raman spectrum and Dra. D.F. Parra for help with the manuscript and fruitful discussions.

References

[1] G. Blasse, B.C. Grabmaier, Luminescence Materials, Springer-Verlag, Heidelberg, 1994.
[2] T. Jüstel, H. Nikol, C. Ronda, Angew. Chem. Int. Ed. 37 (1998) 3084;
C.R. Ronda, T. Jüstel, H. Nikol, J. Alloys Compounds 275–277 (1998) 669.
[3] A.O. Yoshimasa, in: Hiap L. Ong (Ed.), Eletroluminescent Display, Vol. 1, World Scientific, Singapore, 1995.
[4] W.T. Carnall, G.L. Goodman, K. Rajank, R.S. Rana, J. Chem. Phys. 90 (1989) 3443.
[5] J. Hölsä, P. Porcher, J. Chem. Phys. 75 (5) (1981) 2108.
[6] M.A. Bizeto, V.R.L. Constantino, H.F. Brito, J. Alloys Compounds 311 (2000) 159.
[7] O.A. Serra, E.J. Nassar, C.A. Kodaira, C.R. Neri, P.S. Calefi, I.L.V. Rosa, Spectrochim. Acta A 54 (1998) 2077.
[8] J.-C.G. Bünzli, G.R. Choppin (Eds.), Lanthanide Probes in Life, Chemical and Earth Sciences: Theory and Practice, Elsevier, Amsterdam, 1989 (Chapter 7).
[9] J.C. Krupa, J. Alloys Compounds 225 (1995) 1.
[10] R.E. McDonald, M.J. Vogel, J.W. Brookman, IBM J. Res. Dev. 6 (1962) 363.
[11] H.J. Borchardt, J. Chem. Phys. 39 (3) (1963) 504.
[12] D.H. Templeton, A. Zalkin, Acta Crystallogr. 16 (1963) 762.
[13] A. Safari, Y.H. Lee, A. Halliyal, R.E. Newnham, Am. Ceram. Soc. Bull. 66 (4) (1987) 668.
[14] E.C. Paris, E.R. Leite, E. Longo, J.A. Varela, Mater. Lett. 37 (1998) 1.
[15] C.E. Millar, L. Pedersen, W.W. Wolny, Ferroelectrics 133 (1992) 271.
[16] M.U. Pechini, US Patent No. 3330697, 1967.
[17] O.A. Serra, S.A. Cicillini, R.R. Ishiki, J. Alloys Compounds 303–304 (2000) 316.
[18] W. Liu, G.C. Farrington, F. Chaput, B. Dunn, J. Eletrochem. Soc. 143 (3) (1996) 879.
[19] M. Kakihana, M. Arima, M. Yoshimura, N. Ikeda, Y. Sugitani, J. Alloys Compounds 283 (1999) 102.
[20] S.W. Kwon, S.B. Park, G. Seo, S.T. Hwang, J. Nucl. Mater. 257 (1998) 172.
[21] P. Pramanik, Bull. Mater. Sci. 22 (3) (1999) 335.
[22] V.M. Amosov, V.E. Plyushev, Russ. J. Inorg. Chem. 12 (5) (1967) 595.
[23] K. Nassau, H. Levinstein, G.M. Loiacono, J. Phys. Chem. Solids 26 (1965) 1805.
[24] L.J. Burcham, I.E. Wachs, Spectrochim. Acta A 54 (1998) 1355.
[25] H.F. Brito, G.K. Liu, J. Chem. Phys. 112 (9) (2000) 4334.
[26] G. Blasse, S. Kemmler-Sack, Phys. Chem. 87 (1983) 352.
[27] T. Yamase, T. Kobayashi, M. Sugeta, H. Naruke, J. Phys. Chem. A 101 (1997) 5046.
[28] S. Kubota, M. Izumi, H. Yamane, M. Shimada, J. Alloys Compounds 283 (1999) 95.
[29] L. Makalik, J. Hanuza, B. Makalik, W. Strek, J. Legendziewicz, Eur. J. Solid State Inorg. Chem. 33 (1996) 397.
[30] F. Shi, J. Meng, Y. Ren, Q. Su, J. Phys. Chem. Solids 59 (1) (1998) 105.
[31] W.H. Fonger, C.W. Struck, J. Chem. Phys. 52 (12) (1970) 6364.
[32] F. Shi, J. Meng, Y. Ren, Q. Su, J. Mater. Chem. 7 (5) (1997) 773.
[33] G.F. de Sá, O.L. Malta, C.M. Donegá, A.M. Simas, R.L. Longo, P.A. Santa-Cruz, E.F. Silva Jr., Coord. Chem. Rev. 196 (2000) 165.
[34] O.L. Malta, H.F. Brito, J.F.S. Menezes, F.R.G. Silva, S. Alves Jr., F.S. Farias Jr., A.V.M. de Andrade, J. Lumin. 75 (1997) 255.
[35] H.F. Brito, O.L. Malta, J.F.S. Menezes, J. Alloys Compounds 303 (2000) 336.
[36] O.L. Malta, H.F. Brito, J.F.S. Menezes, F.R.G. Silva, C.M. Donegá, S. Alves Jr., Chem. Phys. Lett. 282 (1998) 233.
[37] O.L. Malta, W.M. de Azevedo, E.G. de Araújo, G.F. de Sá, J. Lumin. 26 (1982) 337.
[38] W.T. Carnall, H. Crosswhite, H.M. Crosswhite, Energy Structure and Transition Probabilities of the Trivalent Lanthanides in LaF3, Argonne National Laboratory Report, unnumbered, 1977.
[39] Y.R. Do, Y.D. Huh, J. Electrochem. Soc. 147 (11) (2000) 4385.
[40] C.W. Struck, W.H. Fonger, J. Lumin. 1 (2) (1970) 456.
[41] G.L. Baugis, H.F. Brito, W. Oliveira, F.R. Castro, E.F. Sousa-Aguiar, Microspor. Mesopor. Mater. 49 (2001) 179.